Nanoscale

PAPER

View Article Online
View Journal | View Issue

Check for updates

Cite this: *Nanoscale*, 2019, **11**, 3958

A comparative study demonstrates strong size tunability of carrier–phonon coupling in CdSe-based 2D and 0D nanocrystals†

Riccardo Scott,‡[a] Anatol V. Prudnikau, §[b] Artsiom Antanovich,[b] Sotirios Christodoulou,[c] Thomas Riedl,[d] Guillaume H. V. Bertrand,[e,f] Nina Owschimikow,[a] Jörg K. N. Lindner,[d] Zeger Hens,[g] Iwan Moreels,[g,f] Mikhail Artemyev,[b] Ulrike Woggon[a] and Alexander W. Achtstein *‡[a]

In a comparative study we investigate the carrier–phonon coupling in CdSe based core-only and hetero 2D as well as 0D nanoparticles. We demonstrate that the coupling can be strongly tuned by the lateral size of nanoplatelets, while, due to the weak lateral confinement, the transition energies are only altered by tens of meV. Our analysis shows that an increase in the lateral platelet area results in a strong decrease in the phonon coupling to acoustic modes due to deformation potential interaction, yielding an exciton deformation potential of 3.0 eV in line with theory. In contrast, coupling to optical modes tends to increase with the platelet area. This cannot be explained by Fröhlich interaction, which is generally dominant in II–VI materials. We compare CdSe/CdS nanoplatelets with their equivalent, spherical CdSe/CdS nanoparticles. Universally, in both systems the introduction of a CdS shell is shown to result in an increase of the average phonon coupling, mainly related to an increase of the coupling to acoustic modes, while the coupling to optical modes is reduced with increasing CdS layer thickness. The demonstrated size and CdS overgrowth tunability has strong implications for applications like tuning carrier cooling and carrier multiplication – relevant for solar energy harvesting applications. Other implications range from transport in nanosystems *e.g.* for field effect transistors or dephasing control. Our results open up a new toolbox for the design of photonic materials.

Received 22nd November 2018,
Accepted 28th January 2019

DOI: 10.1039/c8nr09458f

rsc.li/nanoscale

Open Access Article. Published on 30 January 2019. Downloaded on 3/28/2024 5:50:57 PM.
This article is licensed under a Creative Commons Attribution-NonCommercial 3.0 Unported Licence.

Introduction

Optoelectronic properties of semiconductor nanoparticles attract increasing interest because of their promising application potential. Particularly 2D semiconductors in the form of nanoplatelets and sheets[1–6] receive growing attention due to fast radiative lifetimes[7,8] related to strong exciton correlation and the giant oscillator strength effect[4,9,10] allowing high quantum yields,[11,12] promising lasing properties[13–15] and high two-photon absorption.[15–17] Furthermore, their directed emission[18] and polarization[19] and well-width dependent high dark–bright splitting[20,21] of 3–6 meV are of direct interest. High exciton binding energies (of >100 meV) have been predicted and measured,[4,14,22,23] confirming the presence of robust excitons even at room temperature. First predictions have suggested strong tunability of the emission spectra and decay times for platelets and their heterostructures.[24–27] Applications of these nanoparticles for efficient field effect devices[28] or strong electro-absorption response[22,29,30] have been demonstrated.

In recent years, nanoplatelet heterostructures have attracted growing attention due to various properties, which can be engineered in these heterostructures.[11,31–35] On the other hand the opto-electronic properties of core/shell quantum dots are still an active research field.[36–43] First indications have been found that nanoplatelets can exhibit unusually small exciton–phonon coupling.[4] The authors have investigated the

[a]*Institute of Optics and Atomic Physics, Technical University of Berlin, Strasse des 17. Juni 135, 10623 Berlin, Germany. E-mail: achtstein@tu-berlin.de*
[b]*Research Institute for Physical Chemical Problems of Belarusian State University, 220006 Minsk, Belarus*
[c]*ICFO-Institut de Ciencies Fotoniques, 08860 Castelldefels, Barcelona, Spain*
[d]*Department of Physics, Paderborn University, Warburger Strasse 100, 33098 Paderborn, Germany*
[e]*CEA Saclay, 91191 Gif-sur-Yvette, France*
[f]*Istituto Italiano di Tecnologia, Via Morego 30, 16163 Genova, Italy*
[g]*Department of Chemistry, Ghent University, Krijgslaan 281 – S3, 9000 Gent, Belgium*
†Electronic supplementary information (ESI) available. See DOI: 10.1039/C8NR09458F
‡These authors contributed equally to this work.
§Current address: Physical Chemistry, TU Dresden, Bergstraße 66b, 01062 Dresden, Germany.

This journal is © The Royal Society of Chemistry 2019

Open Access Article. Published on 30 January 2019. Downloaded on 3/28/2024 5:50:57 PM.
This article is licensed under a Creative Commons Attribution-NonCommercial 3.0 Unported Licence.

temperature-dependent recombination dynamics, bandgap and quantum yield in 2D CdSe–CdS core–shell platelets,[12] which exhibit a strong thickness dependence. A detailed, comparative study of the (lateral) size and shape dependence of exciton–phonon coupling in different structures like 0D dots and 2D platelets with and without a shell is still missing. Therefore, we investigate in this manuscript at first the size dependent exciton–phonon coupling in core-only CdSe nanoplatelets. Furthermore, we compare the results with CdSe/CdS core/shell nanoplatelets, as well as topologically similar CdSe/CdS heterostructures in the form of CdSe/CdS core/shell quantum dots based on an analysis of the temperature dependent emission line width and bandgap renormalization. We show that the exciton–phonon coupling of these structures can be tuned over about an order of magnitude by varying the lateral size of core only platelets or introducing a CdS shell atop of CdSe quantum dots or platelets, where we compare 0D and 2D systems.

Experimental

4.5 monolayer (ML) zinc blende (ZB) CdSe nanoplatelet samples with different average lateral sizes of 17 × 6 nm^2 to 41 × 13 nm^2 and 4.5 monolayer (ML) thickness were synthesized according to ref. 3 and 44 (see Methods) and characterized by transmission electron microscopy (TEM). To produce CdSe/CdS core/shell nanoplatelets CdSe core-only nanoplatelets with 17 × 11 nm^2 size were coated with 1 to 3 ML CdS by a layer by layer growth technique,[45] see Methods. The final lateral size of CdSe-3 ML CdS core/shell platelets was 22 × 18 nm^2. The samples were embedded in a poly(laurylmethacrylate-*co*-methylmethacrylate) co-polymer on fused silica substrates. Zinc-blende CdSe 4 nm (diam.) core and 2–5 ML CdS shell quantum dots were synthesized according to ref. 40 and 46 and deposited in the PBMA polymer on quartz substrates. The samples were mounted in a CryoVac Micro cryostat. A 150 fs, 75.4 MHz repetition rate Ti:Sa laser at 420 nm was used for confocal exci-

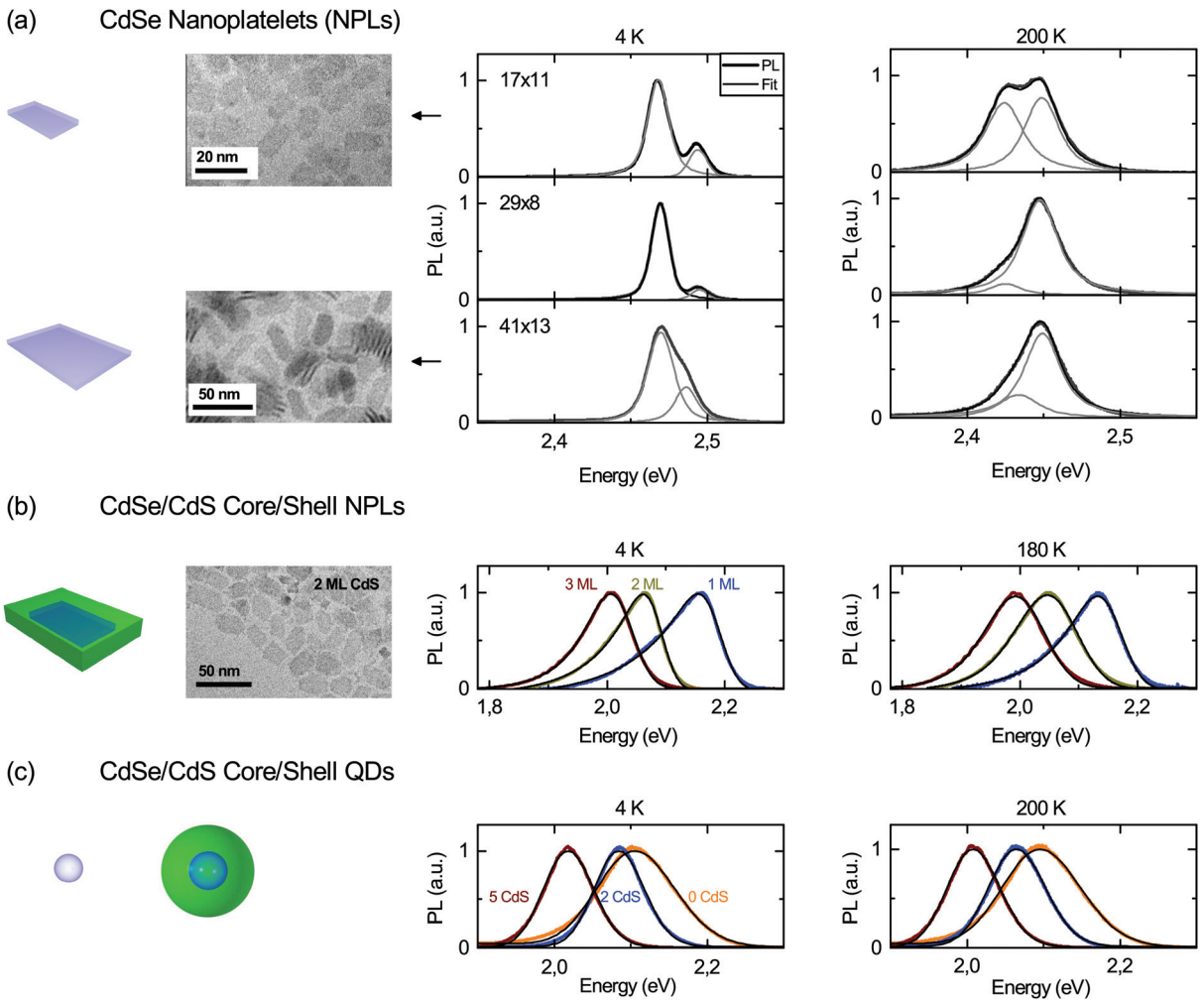


Fig. 1 PL emission of (a) 4.5 ML core-only platelets with varying lateral sizes, (b) CdSe 1 to 3 ML (CdS) CdSe/CdS core/shell nanoplatelets, and (c) CdSe/CdS core/shell quantum dots at 4 K and 180 or 200 K as well as representative TEM images. Clearly a splitting can be observed for the core-only nanoplatelets (a) at low temperatures in line with ref. 7. PL from core-only platelets is fitted with two Voigt profiles, and core/shell particles with a modified Gaussian (black lines atop experimental curves).

Open Access Article. Published on 30 January 2019. Downloaded on 3/28/2024 5:50:57 PM.
This article is licensed under a Creative Commons Attribution-NonCommercial 3.0 Unported Licence.

tation with a 0.4 NA objective (≈0.2 W cm^{-2} CW equivalent excitation density) for the nanoplatelets and a 442 nm He:Cd laser for the core/shell dot samples with comparable excitation density. Time integrated detection was realized by using a Horiba IHR550 spectrometer with an attached LN_2 cooled CCD.

Results and discussion

Fig. 1 shows temperature dependent PL spectra for two exemplary temperatures of (a) 4.5 ML ZB CdSe core-only platelets with varying lateral sizes, (b) CdSe-*n*ML CdS (n = 0, 1, 2, 3) ZB nanoplatelets (17 × 11 nm^2 core size) and (c) of 4 nm (diameter) ZB CdSe core and 2, 3, and 5 ML CdS shell CdSe–CdS dots.

The increasing redshift with shell thickness (at fixed temperature) in (b) and (c) can be attributed to a lowering of the confinement related to lower conduction and valence band offsets resulting in increasing delocalization of the CdSe core exciton into the CdS shell of the heterostructures. In CdSe–CdS core–shell nanoplatelets it has been shown that still type I band alignment is maintained,[12] so that our observed redshift here is not an effect of strongly different spatial electron and hole localizations, but the band alignment.

CdSe core-only nanoplatelets

We first concentrate on the CdSe core-only nanoplatelets. In line with recent results[7] we observe for the core-only platelets a double emission with 20–40 meV energy spacing. Fig. 2(a) shows the temperature dependence of the centers of the double emission, obtained from Voigt fits (shown in Fig. 1) in the range of 4 to 300 K. We refer to the lower energy peak as the ground state (GS) and the higher one as the excited state (ES), without any presumptive attribution to the nature of the states. We would like to point out here that their origin – excited and ground state excitons, an exciton plus trion or an exciton plus an LO phonon replica – is still under debate.[7,21,47] However, this does not affect our bandgap analysis, since both states show the same temperature dependence of the bandgap (Fig. 2a). Hence, we concentrate on the results for the energetically higher emission for the core-only sample. Furthermore, studying the emission dynamics of CdSe nanoplatelets, Biadala *et al.*[20] recently demonstrated a dark–bright state fine structure with energy splittings of about 5 meV. Even for the presence of a higher bright and a lower dark state, Shornikova *et al.*[34] have shown that the quasi dark exciton state does not contribute relevantly to the PL emission above 10 K resulting in no relevant impact on our measurements.

An initial observation for the nanoplatelets (Fig. 2a) is the steeper redshift (high temperature slope) for increasing lateral platelet size (area). At first we concentrate on the lateral size dependence of the temperature-dependent bandgap shift and exciton phonon coupling. Fits to a semi-empirical model for the bandgap shift are given by[48,49]

$$E_{\max} = E_0 - a_{\mathrm{ep}}\left(1 + \frac{2}{e^{\theta/T} - 1}\right), \qquad (1)$$

where a_{ep} an exciton–phonon coupling strength and $\theta = \langle\hbar\omega\rangle/k_{\mathrm{B}}$ an average phonon temperature are indicated as solid lines in Fig. 2(a). The results for the zero temperature bandgap E_0, a_{ep} and θ are displayed in Fig. 2(b)–(d).

Using eqn (1) allows the analysis of the impact of lateral confinement on the zero temperature excitonic bandgap E_0 of CdSe nanoplatelets at low temperature as shown in Fig. 2(b). Starting from the approximate expression for the confinement energy related bandgap shift ΔE of an infinitely deep semiconductor quantum box in x, y and transversal z direction the observed bandgap is

$$E_{\mathrm{g}} = E_{\mathrm{g,bulk}} - E_{\mathrm{B}} + \frac{{n_z}^2\pi^2\hbar^2}{2\mu_z {L_z}^2} + \frac{\pi^2\hbar^2}{2M_{x,y}}\left[\left(\frac{n_x}{L_x}\right)^2 + \left(\frac{n_y}{L_y}\right)^2\right] \qquad (2)$$

where $E_{\mathrm{g,bulk}}$ is the bulk bandgap, E_{B} is the exciton binding energy, and μ is the reduced exciton mass. $M_{x,y}$ is the exciton mass and $n_{x,y,z}$ is the quantum number in the x,y,z direction. We note that NPLs are strongly confined in the z-direction

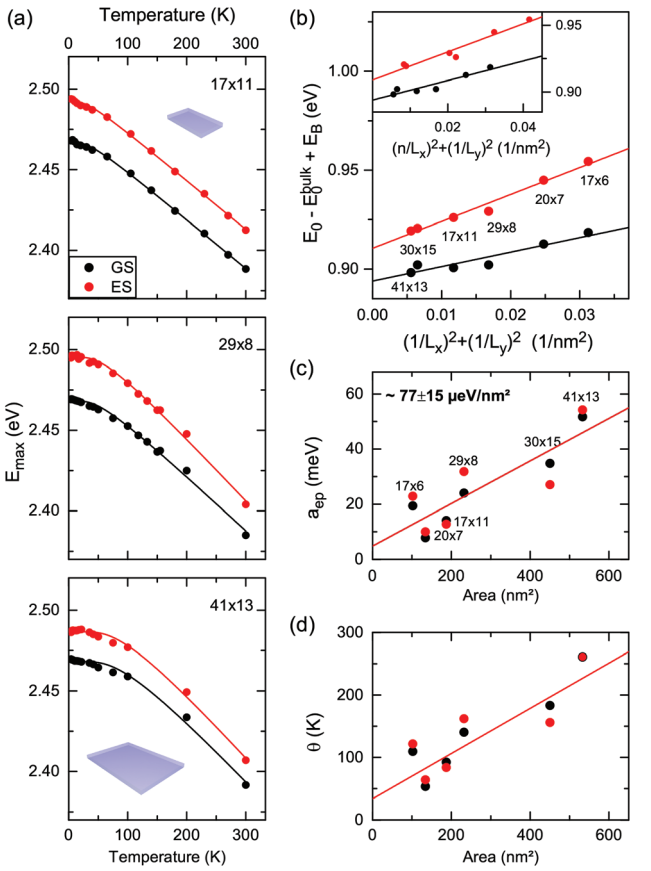


Fig. 2 (a) Temperature dependent excitonic bandgap of 4.5 ML core-only nanoplatelets with different lateral sizes obtained from the Voigt fits in Fig. 1. Solid lines are fits according to eqn (1) in order to obtain: (b) lateral confinement part of the zero temperature excitonic bandgap *versus* $(1/L_x)^2 + (1/L_y)^2$ with $L_{x,y}$ the lateral platelet dimensions. The inset shows the same data plotted against $(n/L_x)^2 + (1/L_y)^2$, with n = 1 for the GS and n = 2 for the ES. (c) The exciton–phonon coupling a_{ep} and (d) the average phonon temperature θ.

This journal is © The Royal Society of Chemistry 2019

Open Access Article. Published on 30 January 2019. Downloaded on 3/28/2024 5:50:57 PM.
This article is licensed under a Creative Commons Attribution-NonCommercial 3.0 Unported Licence.

(quantization of relative motion), while weakly confined in in-plane directions[7] (quantization of center of mass motion). Under the assumption of a lowest electron and hole state transition $n_{x,y,z} = 1$ in all directions and taking the x-direction as the long side of the rectangular platelet, the first excited state would be $(n_x,n_y,n_z) = (2,1,1)$ and the ground state (1,1,1) (see also ESI† for a detailed discussion). The exciton binding energy depends only weakly on the lateral size[7] and can be assumed to be constant. The z-quantization energy is also constant for fixed thickness as well as the bulk bandgap $E_{g,bulk}$.

A plot of $dE = E_g - E_{g,bulk} + E_B$ *versus* $(1/L_x)^2 + (1/L_y)^2$ assuming (1,1,1) for the upper and lower emission states from Fig. 1 is shown in Fig. 2. A linear dependence is fitted in this plot ($R^2 = 0.98$). The slope $\pi^2\hbar^2/2M_{x,y}$ corresponds to the quasi-particle (*e.g.* exciton) mass. The different slopes for the upper and lower emission indicate different masses of the emitting species, inferring different species or ground and excited states. A plot under the assumption of ground state (GS) (1,1,1) and excited state (ES) (2,1,1) excitons leads to less good correlation ($R^2 = 0.94$) for a fit to the shifts *vs.* $(n/L_x)^2 + (1/L_y)^2$ and is shown in the inset of Fig. 2(b). However, a definite answer to which of the two models applies cannot be given based on the lateral confinement. As shown in the ESI,† comparing $M_{x,y}$ to the literature values of the effective carrier masses in ZB CdSe for excitons, positive and negative trions and biexcitons and the ES and GS hypothesis also do not result in a final attribution. One possible scenario for the double emission discussed based on the displayed results here is an exciton and biexciton state.

Fig. 2(b) also allows us to extrapolate the energy difference of the two states for laterally infinite platelets or sheets as the difference of the intersection points of the fit curves with the ordinate. The extrapolation to laterally infinite platelets with vanishing lateral confinement results in an energy spacing of 17 meV. From the two fit curves in Fig. 2(b) the area dependent energy spacing can be given as

$$\Delta E[\mathrm{eV}] = 1.600 \times 10^{-2} + 0.652 \cdot (1/{L_x}^2 + 1/{L_y}^2), \qquad (3)$$

if the corresponding lengths are given in nm.

Fig. 2(c) shows the electron–phonon coupling parameter a_{ep} obtained from the temperature-dependence of the bandgap according to eqn (1). For both, the ES and GS, a_{ep} tends to increase linearly with the platelet area -with some scattering of the data, perhaps due to not identical sample quality. A linear fit to all data (with non-zero offset) yields a slope of 77 ± 15 μeV nm^{-2}.

A possible explanation for this linear increase is the coherent delocalization of the 2D excitons over the whole nanoplatelets. The number of unit cell dipole moments contributing to the exciton transition dipole moment increases with the platelet area *via* the giant oscillator strength effect (GOST).[50] These elementary dipole moments coherently add up to the transition dipole moment of the exciton, which then couples to the phonon modes, leading to a linear increase of the coupling strength with the platelet area. Clear indications for this coherent delocalization over the whole nanoplatelet and the resulting increase of the transition rates in our size range of nanoplatelets have been found in ref. 8 and 10. In particular the scaling of the transition rates with the platelet area leads to a quadratic area (volume) scaling of the two photon absorption cross section with the lateral platelet size as well as a constant intrinsic absorption in the continuum. We remark that these effects of coherent delocalization are observed, as the nanoplatelets are atomically flat systems[51] due to their anisotropic colloidal synthesis. In contrast epitaxial quantum wells suffer *e.g.* from interface roughness effects, which limit the spatial coherence of excitons more strongly.

We remark that the trend of increased exciton–phonon coupling is also observed, if a_{ep} is converted in the dimensionless Huang–Rhys parameter S, often used to quantify the strength of phonon coupling, and that the resulting values are comparable to laterally quasi infinite 2D transition dichalcogenide materials[52,53] (see the ESI†).

The linear increase of a_{ep} shown in Fig. 2(c) allows for a control of electron–phonon interaction and the accompanied temperature-dependent bandgap red shift with the platelet area. Additionally, it directly implies control over dephasing in the system, as discussed later. Furthermore, this degree of freedom is practically independent of the emission energy of the system – the bandgap shifts are less than 30 meV and small compared to the ~2.5 eV band gap that is controlled by the platelets' thickness.

Fig. 2(d) shows the average phonon temperature θ. It corresponds to a weighted average phonon energy of acoustic and optical modes. The observed increase of θ with lateral size may be related to alterations in the average coupling to acoustic and optical phonons. It can be shown (later) that the coupling to acoustic phonons in 2D systems scales with $1/A$ (A being the platelet area), so that the contribution of acoustic modes is reduced with increasing platelet size. At the same time the contribution of optical modes increases. Since these exhibit energies higher than acoustic modes, the average phonon energy (temperature) increases with lateral size.

CdSe/CdS core/shell nanoplatelets and dots

In the following section we concentrate on the CdSe/CdS core/shell nanoplatelet and quantum dot samples. Fig. 3(a) and (b) compare the temperature dependent excitonic band gaps E_{max} deduced from fits to the PL (Fig. 1) and fitted with eqn (1). The CdSe/CdS platelet values presented here for comparison are in agreement with those recently obtained on CdSe/CdS NPLS.[12] Fig. 3(c) and (d) show the resulting exciton–phonon coupling a_{ep}, and (e) and (f) the average phonon temperatures θ.

As seen in the case of core-only platelets in Fig. 2(c), the exciton–phonon interaction a_{ep} is linear in the platelet area A. On the other hand, the density of states in a 2D system is proportional to $1/d$ (inverse thickness) and alters the interaction strength. For this reason, we plot in Fig. 3(c) the interaction strength per CdSe nanoplatelet area *versus* $1/d_{CdS}$, the CdS

Open Access Article. Published on 30 January 2019. Downloaded on 3/28/2024 5:50:57 PM.
This article is licensed under a Creative Commons Attribution-NonCommercial 3.0 Unported Licence.

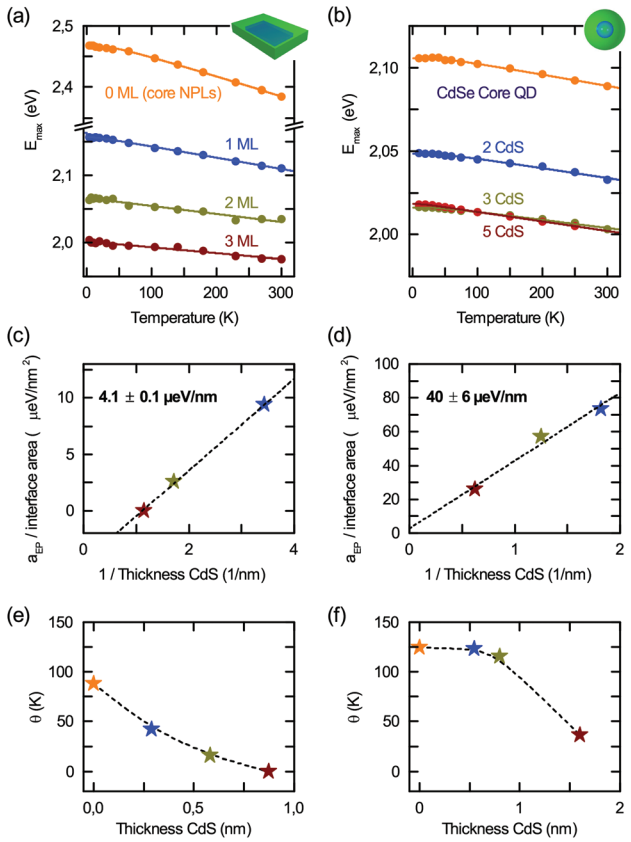


Fig. 3 Temperature dependent excitonic bandgaps deduced from fits to PL in Fig. 1 for 4.5 ML core/shell nanoplatelets (a) and 4 nm diameter CdSe core/shell dots (b) with 0–3 ML and 0–5 ML CdS shell, respectively. Exciton–phonon coupling a_{ep} per interface area for the platelets (c) and dots (d) *versus* the inverse CdS thickness. For the platelets the system has two interfaces as well as their average phonon temperature θ (e) + (f) determined from fits in (a) and (b).

layer thickness. The slope is equivalent to plotting a_{ep} per surface area ($2A$) *versus* the inverse total CdS thickness of $2d_{CdS}$. For quantum dots shown in Fig. 3(d) we use the interface area given by $4\pi(d/2)^2$, with the core diameter d. We observe a linear dependence with a slope of 4.1 ± 0.1 μeV nm^{-1} for the core/shell platelets and 40 ± 6 μeV nm^{-1} for the core/shell dots.

Thus – in addition to the lateral size – a CdS shell also allows for controlling the exciton–phonon interaction in CdSe nanoplatelets and dots, in line with the first indications in ref. 12 and 42 in PL and Raman spectroscopy. Interestingly, the same concept applies to topologically similar core/shell quantum dots, which can be considered as spherical 2D CdSe/CdS interface structures, where the interaction is proportional to the interaction (interface) area. A decreasing coupling with CdS shell thickness is consistent with the results of Lin *et al.*,[42] who observed in Raman measurements that the Huang–Rhys factor for LO-phonon coupling tended to decrease upon introduction of a shell. There, a model assuming a Fröhlich-only mechanism was not able to reproduce this trend. They offer surface charging and related S- and P-type wavefunction mixing as a possible mechanism for increasing the e–h separation and counteracting the Fröhlich coupling trend. Finally, considering the slopes in Fig. 3(c) and (d), the exciton–phonon interaction per unit area in CdSe/CdS nanoplatelets is lower than that in CdSe/CdS dots. We remark that as the platelets exhibit type I band alignment,[12] there are no effects of spatially indirect exciton formation, which alters the coupling to phonons. For CdSe–CdS dots type I band alignment is also suggested,[54] but is still under discussion.[55]

The performed renormalization by the surface area is also substantiated by the results of Takagahara *et al.*[56] for spherical CdSe core-only quantum dots. They found a $1/r^2 \propto 1/A$ dependence for coupling in dots, where r is the crystallite radius. In Fig. 3(e) and (f), we further observe a reduction of the average phonon temperature with increasing CdS thickness. While the starting point for core-only samples is comparable for platelets and dots, the decrease is faster for platelets. This difference can be attributed to the different phonon densities of states for the 2D system and the spherical CdSe/CdS hetero system, so that a different scaling of the coupling to acoustic and optical modes may be the reason for these findings. As for the core-only platelets we recalculated from Fig. 3(c)–(f) the Huang–Rhys parameter S (see Fig. S1 in the ESI†) and found that S decreases with the CdS thickness in line with Fig. 3(c) and (d).

Based on an analysis of the emission line width, we will now investigate the acoustic and optical phonon coupling in more detail.

Linewidth

Fig. 4(a) shows the temperature dependent linewidth (FWHM) obtained from the log-normal function fits to the PL spectra in Fig. 1. We fit the temperature dependence with the well known expression

$$\Delta(T) = \Delta_0 + \Delta_{AC} T + \Delta_{LO} \frac{1}{e^{E_{LO}/k_B T} - 1}, \quad (4)$$

where Δ_0 is the sum of the (temperature independent) inhomogeneous and zero-temperature linewidth. Δ_{AC} is the coupling to acoustic and Δ_{LO} the coupling to LO phonons, with the LO phonon energy $E_{LO} = 25.4$ meV.[57] (See also the ESI† for the discussion of line width related effects.)

The results for core-only nanoplatelets are shown in Fig. 4(b) and (c). While there is a clear trend of a reduction of Δ_{AC} with the platelet area, only a by trend increase is observed for Δ_{LO}. Both trends are in line with the results in Fig. 2(d), where with increasing lateral size LO phonons provide increasingly major contribution to the average phonon temperature. θ approaches the LO phonon temperature of ~300 K (equal to 25.4 meV) for large platelets. The demonstrated strong area scaling of the acoustic phonon interaction can be understood from the underlying theory of deformation potential interaction[58,59] of acoustic phonons. According to Fermi's golden rule the transition rate Γ is proportional to the absolute value squared of transition matrix element. The effective deformation potential coupling $u_{DP} = (D_e - D_h)(\hbar q/2\Omega\rho\nu_s)^{1/2}$ relates

This journal is © The Royal Society of Chemistry 2019

Open Access Article. Published on 30 January 2019. Downloaded on 3/28/2024 5:50:57 PM.
This article is licensed under a Creative Commons Attribution-NonCommercial 3.0 Unported Licence.

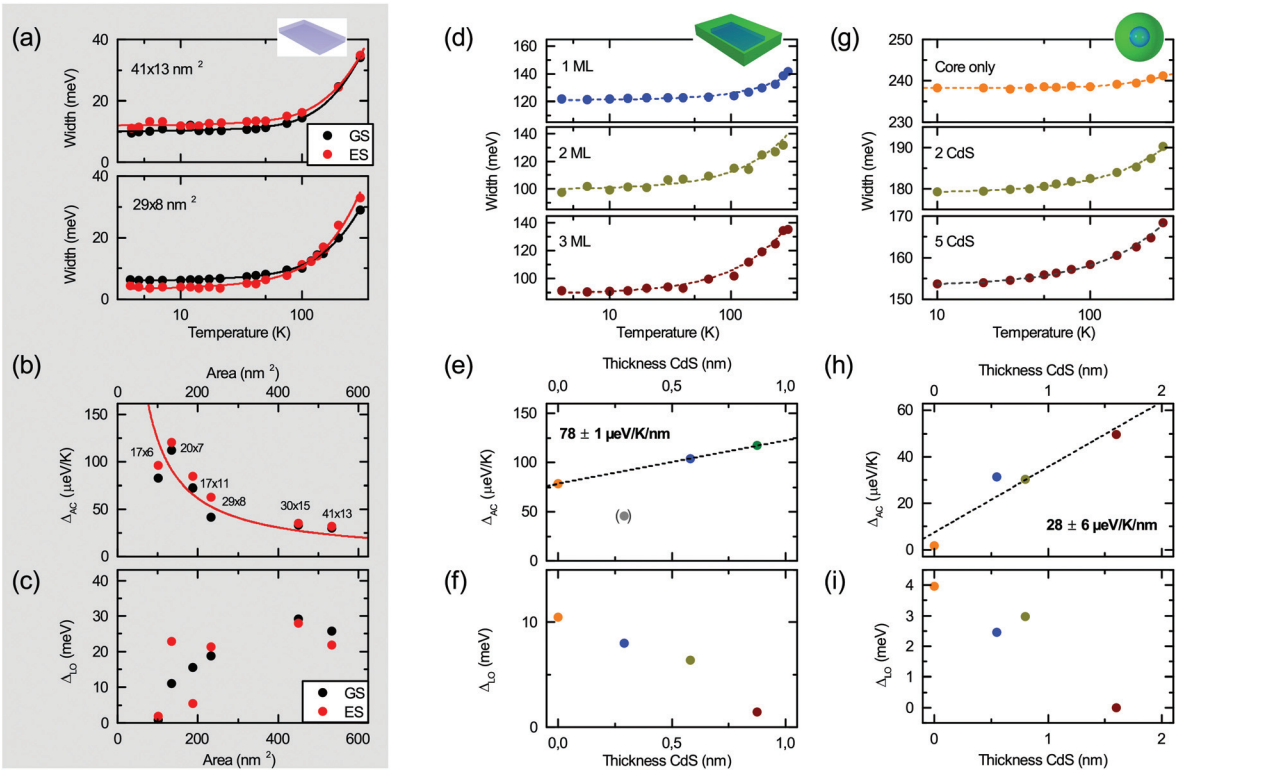


Fig. 4 Temperature dependent line width of CdSe platelets (a), CdSe/CdS nanoplatelets (17 × 11 nm^2 CdSe core) (d) and nano-dots with 4 nm core size (g), with fits to eqn (4). Resulting acoustic Δ_{AC} (b) and LO phonon Δ_{LO} (c) contribution to the linewidth as a function of the nanoplatelet area. (b) shows a 1/*A* fit according to eqn (5). (e, h) and (f, i) acoustic Δ_{AC} and LO phonon Δ_{LO} contribution for core/shell platelets and dots *versus* the CdS layer thickness.

the phonon wave number q (absolute value of the wave vector), the volume Ω of the structure under consideration, the density ρ, the sound velocity v_s and the deformation potential difference of $D_e - D_h$ of electrons and holes. The corresponding matrix element is $M_{k,k'} = (D_e - D_h)(\hbar q/2\Omega\rho v_s)^{1/2} f(q)\delta_{k,k'+q}$. $f(q)$ is the form factor that can be shown[59] to be $(1 + (qa_B/4))^{-3/2}$ for a hydrogen (S-)like lowest envelope function and small acoustic phonon wave vectors, as estimated from ref. 7 and 60.

Due to Fermi's golden rule the transition rate Γ scales with the square of u_{DP}. In our platelets with dimensions $L_{x,y,z}$ and volume $\Omega = L_xL_yL_z$, the quantized phonon wave vector is $q = \pi(1/L_x^2 + 1/L_y^2 + 1/L_z^2)^{1/2}$. Following ref. 61 and 59, and assuming small acoustic phonon wave vectors (as *e.g.* also shown in ref. 62), the third contribution is the dominant one and is given by the *z*-breathing mode frequency (taken from ref. 60) since $L_x,L_y \gg L_z$. The contribution of acoustic phonon scattering to the homogeneous line width is $\Delta_{acoust} = 2\hbar\Gamma$.[10] Since according to eqn (4) $\Delta_{acoust}(T) = \Delta_{AC}T$, this leads, apart from a scaling factor C_{DP}, to the following dependency

$$\Delta_{AC} = C_{DP}^2 \frac{\left(L_x^{-2} + L_y^{-2} + L_z^{-2}\right)^{1/2}}{L_xL_yL_z} \approx C_{DP}^2 \frac{1}{L_xL_yL_z^2} = C_{DP}^2 \frac{1}{AL_z^2}, \quad (5)$$

where the last line is an approximation for $L_x,L_y \gg L_z$ and fixed well width L_z. Hence, we can understand the decrease of the acoustic phonon coupling with increasing platelet area as shown in Fig. 4(b). A fit to the function above is indicated. $C_p^2 = 2\pi^2\hbar k_B(D_e - D_h)^2/\rho E_{ph}^2$ is a material dependent proportionality constant, resulting from the considerations discussed above. Using an effective exciton mass from ref. 7, a ZB CdSe sound velocity of v_s = 2.26 km s^{-1},[60,63] an acoustic phonon energy of E_{ph} = 3.42 meV calculated[60] from the sound velocity, a platelet thickness of 4.5 ML and a mass density of ρ = 5.66 g cm^{-3},[60] we obtain from the fit to eqn (5) $|D_e - D_h|$ = 3.03 ± 0.3 eV. This value is in excellent agreement with a value of −2.87 eV calculated from elastic constants based on DFT results[64] and results on ZB CdSe.[65] It further shows that the deformation potential is unaltered by the strong anisotropic size quantization in CdSe nanoplatelets. The agreement of the deformation potentials directly justifies our approach, the validity of our fits to the emission lines and the assumptions of our model. It proves that we demonstrate for the first time an independent control of the acoustic phonon coupling or dephasing from the transition energy in a nanosystem. As the homogeneous line-width is shown to be acoustic phonon scattering limited, we obtain a direct control over dephasing in our system *via* the lateral platelet area. A tuning range of more than a factor of four with increasing values for small platelets

Open Access Article. Published on 30 January 2019. Downloaded on 3/28/2024 5:50:57 PM.
This article is licensed under a Creative Commons Attribution-NonCommercial 3.0 Unported Licence.

gives great prospects that for smaller platelets even higher Δ_{AC} values can be obtained.

Slight deviations of the actual platelets from the fit curve in Fig. 4(b) may be related to slight variation of sample quality or size determination by TEM.

We remark that the observed trend of a decrease of acoustic phonon coupling with nanostructure size is in-line with calculations by Kelley[66] and Takagahara *et al.*[56] for spherical CdSe quantum dots. With increasing size the exciton coupling to acoustic phonons was observed to decrease due to decreasing deformation potential coupling. Our results for large platelets are comparable to large dots, for which Takagahara *et al.* found the coupling to be about 7 μeV K^{-1}. For small quantum dots, of diameter comparable to the thickness of our 4.5 ML platelets (1.4 nm), they obtained ~100 μeV K^{-1} – in good agreement with the values of smaller platelets as shown in Fig. 4(b). We also note that they found a $1/r^2$ dependence for dots, where r is the crystallite radius. This corresponds to an inverse surface area dependence of the nanocrystal analogous to our findings for the nanoplatelets ($\propto 1/A$).

This inverse relationship between coupling to low energy acoustic modes and platelet area A further substantiates our interpretation of the increase of the average phonon temperature θ as shown in Fig. 2(d) with A. For larger lateral sizes the contribution of low energy acoustic modes decreases due to the reduced coupling while optical modes with higher phonon energies increasingly contribute to the average phonon temperature.

In Fig. 4(c) we further observe a by trend increase of the coupling to LO-phonons with increasing nanoplatelet area. The coupling to optical modes tends to increase with A and then saturate for large platelet areas towards values reported by Chia *et al.* for laterally infinite MBE grown CdSe epilayers (≈20 meV).[67] As the Fröhlich interaction is considered the dominating mechanism[42] for the LO phonon coupling in polar semiconductor nano-structures we briefly investigate whether this can explain the observed complicated behavior directly. The corresponding interaction potential[59] $u_F = -i(e/q)\left(\frac{E_{LO}}{2\Omega\varepsilon_0}\left(\varepsilon_r^{-1} - \varepsilon_\infty^{-1}\right)\right)^{1/2}$ results in a predicted scaling $\Delta_{LO} \propto \left(1/L_x^2 + 1/L_y^2 + 1/L_z^2\right)^{-1} L_x L_y L_z \propto A/2L_z[(L_x - L_y)^2 + A]$, where the first proportionality is an approximation due to $L_x, L_y \gg L_z$ and the last proportionality due to $L_x \sim L_y$ for fixed well width L_z. A nonlinear increase for larger platelet areas is expected for more quadratic nanoplatelets. The observed scatter of data points may be related to the lateral aspect ratio sensitivity (*via* the $(L_x - L_y)^2$ dependence), as the used platelets have varying aspect ratios. However, the actual trend in Fig. 4(c) cannot be fully explained by this simple theory. Another explanation for deviations from the simple scaling theory presented could be a varying defect density which alters the LO phonon coupling, as *e.g.* the number of defect sites scales with the platelet area. A detailed analysis, however, is beyond the scope of this article.

In the following we analyze the cases of CdSe/CdS platelets and dots for varying CdS layer thicknesses. Fig. 4(e) and (f) show the coupling to acoustic and optical modes. Δ_{AC} can be (roughly) approximated with a linear increase with the CdS layer thickness. The 1 ML CdS sample is excluded from the linear fit shown in Fig. 3(e). The trend – which is in line with the reduction of the average phonon temperature in Fig. 3(c + d) *via* increasing coupling to low energy acoustic phonons – may be interpreted in terms of an increase of the interaction volume with increasing shell thickness. In bulk the acoustic branches of the phonon dispersion in CdSe and CdS are quite similar and have a continuous spectrum. Here we have quantized acoustic modes, but the energy spectrum is still quite similar in both materials, which can be seen from the fact that the acoustic sound velocities 2.3 km s^{-1} and 2.6 km s^{-1} for CdSe and CdS (calculated based on ref. 60) are quite similar. Hence there is no strong mode confinement due to the CdSe–CdS interface and to a first approximation the acoustic modes can be considered as to extend over the whole particle, including the CdS shell. In contrast these arguments do not apply to the optical modes, as the energies of LO phonons in CdSe (~210 cm^{-1}) and CdS (~302 cm^{-1}) are well distinct. Hence, an increased shell thickness and wavefunction delocalization may tend to decrease the LO coupling as the core (LO) phonon modes cannot couple to the shell modes and the wavefunction overlap of the exciton with the core mode decreases relatively for stronger delocalization into thicker CdS shells.

A reduction of the coupling to LO phonons is further observed in (f). Lin *et al.*[42] measured a non Fröhlich-like reduction of the coupling (Huang–Rhys factor S) with increasing shell thickness in CdSe/CdS quantum dots – in-line with our result. This seems to be a universal trend in hetero-nanoplatelets and quantum dots. Furthermore, the decreasing coupling to high energy LO-phonons with increasing layer thickness is also reflected in the reduction of the average phonon temperature θ as seen in Fig. 3(e) and (f). This also confirms the consistency of our whole analysis *via* the independent experimental quantities, bandgap and line width.

The same trends of acoustic and optical phonon coupling with CdS shell thickness discussed now for platelets (Fig. 4(e + f)) are also observed for the topologically similar CdSe/CdS dots. On an absolute scale, they show smaller coupling than nanoplatelets. This may stem from smaller transition dipole moments in dots as compared to platelets coupling to phonons, or a not perfect spherical shape of the nanoparticles. The dots are smaller than the nanoplatelets. This may result in a smaller number of acoustic or LO-phonon modes in the system to which the exciton can couple, leading to an overall reduction in CdSe/CdS dots compared to platelets. Furthermore, due to different crystallographic orientations on the dot surface, CdS monolayers are not as ideally smooth as on the platelets, which may result *e.g.* in the larger data point scatter.

The demonstration of the tuneability of exciton–phonon interaction in colloidal quantum-wells by lateral size and shell growth has strong application potential, for example, for tuning carrier cooling, which is relevant *e.g.* in solar energy harvesting applications. Furthermore, carrier multiplication is

 This journal is © The Royal Society of Chemistry 2019

Open Access Article. Published on 30 January 2019. Downloaded on 3/28/2024 5:50:57 PM.
This article is licensed under a Creative Commons Attribution-NonCommercial 3.0 Unported Licence.

a very active field, where carrier cooling and carrier multiplication are competing processes. The former tunes the multicarrier pair generation efficiencies and poses a promising way to boost solar cell efficiencies. Hence 2D materials of finite lateral size, like the nanoplatelets in this manuscript, with a control of the carrier cooling rates are desirable model systems, for both basic understanding of the involved processes as well as optimization of the performance of solar energy converters. Also for transport in nanosystems our results show the feasibility of tuning exciton–phonon interaction, for example in field-effect transistors, varying the lateral size of the structure and *e.g.* tuning from ballistic to diffusive transport. A further interesting implication of our results is that the quantum yield of nanoplatelets with or without a shell, which has been found to be considerably different,[12] will depend on the phonon interaction, which governs exciton cooling and relaxation in non-radiative channels. For large platelets or core/shell platelets with thin shells the average phonon coupling is the highest, so that *e.g.* phonon assisted nonradiative recombination is stronger. These findings can be used for emitters of optimized photoluminescence efficiency. Our results open up a new toolbox for the design of photonic materials.

Conclusion

In summary we have shown that CdSe nanoplatelets possess a lateral confinement of ~30 meV, which can be adjusted *via* the lateral size of the nanoplatelets. We demonstrated that exciton–phonon coupling in CdSe nanoplatelets can be varied strongly *via* the lateral size or the thickness of a CdS shell. The coupling to acoustic phonons decreases with the platelet area by a factor of ~4, in line with deformation potential theory. The resulting −3.03 eV exciton–acoustic phonon deformation potential is in line with theory predictions. The coupling to LO-phonons is observed to decrease with decreasing platelet area. We further demonstrated that a CdS shell results in an increased coupling to acoustic modes and reduced coupling to optical modes for both CdSe–CdS core–shell platelets and quantum dots. The absolute coupling strengths are lower for quantum dots than for nanoplatelets, which may be attributed to the higher transition dipole moments to which the phonon modes couple in nanoplatelets and more phonon modes to couple to in the larger nanoplatelets. We further demonstrated that the average exciton–phonon coupling strength increases linearly with the platelet area for core-only platelets, while it is linear in the interface area *versus* the inverse CdS layer thickness in core/shell platelets as well as in nanodots. As the trends for both core/shell structures are similar, there is a universal mechanism for 2D platelets and similar core–shell dots also exhibiting a 2D interface. Our results regarding the tunability of phonon interaction are of immediate interest for carrier cooling and multiexciton generation, relevant for solar light conversion, for transport and high quantum yield emitters and open up a new toolbox for the design of photonic materials. We remark that further in-depth studies beyond the scope of this article are necessary to give a definite answer to the nature of the two emissive states in CdSe nanoplatelets, however our experimental results presented in this paper are not influenced by this.

Methods

Synthesis and characterization

Nanoplatelets. 4.5 ML-thick CdSe NPls were prepared using a modified procedure based on the protocols described in ref. 3 and 44. 170 mg of cadmium myristate, 12 mg of elemental selenium and 15 ml of octadecene-1 were charged into a three-necked flask. The flask was degassed for 15 minutes, purged with argon and set to heat up to 240 °C. At 190 °C a mixture of 56 mg of cadmium acetate dihydrate and 21 mg of anhydrous cadmium acetate was swiftly added into the reaction mixture. The ratio of anhydrous/hydrate allows tuning the aspect ratio. When the temperature reached 240 °C, the flask was kept at this temperature for 45 s to 2 min. After that, the reaction mixture was cooled to 80 °C and nanocrystals were precipitated with isopropanol and hexane and isolated by centrifugation. The cadmium sulfide shell was deposited onto CdSe NPL cores by a colloidal atomic layer deposition technique.[45] At first, 2 ml of hexane colloidal solution of CdSe NPls were mixed with 2 ml of *N*-methylformamide (NMF). Then 10 μL of 40 wt% ammonium sulfide aqueous solution was added and NPls were transferred into the NMF phase due to the growth of a sulfide surface layer. After 10 minutes of vigorous mixing the hexane layer was discarded and then, in order to remove the excess of sulfur precursor, the NPLs were precipitated with isopropanol, isolated by centrifugation and redispersed in fresh NMF. To ensure complete removal of the unreacted sulfide the precipitation step was repeated twice. In order to complete the deposition of 1 ML of CdS by growing a cadmium layer, 20 μL of 0.1 M solution of cadmium acetate in water were added to the solution of sulfide-covered NPLs in NMF. After 20 minutes of mixing the NPLs were purified from the excess of the cadmium precursor by the precipitation procedure described above. NPLs were then transferred into hexane by adding 10 μL of oleic acid and thorough mixing. Second and third layers were grown by repeating the steps described above.

Zinc-blende CdSe core-only and 2–5 ML CdS shell quantum dots. These were synthesized according to ref. 40 and 46 based on 4 nm CdSe cores and deposited in PBMA polymers on quartz substrates. Sizes and diameters were determined by TEM in all samples.

TEM analysis of all samples was performed through different instruments (Jeol ARM200F operated at 200 kV and Zeiss Leo 906E at 120 kV). At least 50 platelets per sample were used for size determination.

Conflicts of interest

There are no conflicts to declare.

Open Access Article. Published on 30 January 2019. Downloaded on 3/28/2024 5:50:57 PM.
This article is licensed under a Creative Commons Attribution-NonCommercial 3.0 Unported Licence.

Acknowledgements

R. S., U. W. and A. W. A acknowledge the DFG grants WO477-1/32 and AC290-2/1., M. A. the CHEMREAGENTS program, and A. A. the BRFFI grant no. X17KIG-004.

References

1 F. Gerdes, C. Navío, B. H. Juárez and C. Klinke, *Nano Lett.*, 2017, **17**, 4165–4171.
2 J. Joo, J. S. Son, S. G. Kwon, J. H. Yu and T. Hyeon, *J. Am. Chem. Soc.*, 2006, **128**, 5632–5633.
3 S. Ithurria and B. Dubertret, *J. Am. Chem. Soc.*, 2008, **130**, 16504–16505.
4 A. W. Achtstein, A. Schliwa, A. Prudnikau, M. Hardzei, M. V. Artemyev, C. Thomsen and U. Woggon, *Nano Lett.*, 2012, **12**, 3151–3157.
5 Q. Wang, K. Kalantar-Zadeh, A. Kis, J. Coleman and M. Strano, *Nat. Mater.*, 2012, 699–712.
6 A. Steinhoff, M. Florian, A. Singh, K. Tran, M. Kolarczik, S. Helmrich, A. W. Achtstein, U. Woggon, N. Owschimikow, F. Jahnke and X. Li, *Nat. Phys.*, 2018, **14**, 1199.
7 A. W. Achtstein, R. Scott, S. Kickhöfel, S. T. Jagsch, S. Christodoulou, G. H. Bertrand, A. V. Prudnikau, A. Antanovich, M. Artemyev, I. Moreels, A. Schliwa and U. Woggon, *Phys. Rev. Lett.*, 2016, **116**, 116802.
8 J. Planelles, A. W. Achtstein, R. Scott, N. Owschimikow, U. Woggon and J. I. Climente, *ACS Photonics*, 2018, **5**, 3680–3688.
9 S. Ithurria, M. D. Tessier, B. Mahler, R. P. S. M. Lobo, B. Dubertret and A. L. Efros, *Nat. Mater.*, 2011, **10**, 936–941.
10 A. Naeem, F. Masia, S. Christodoulou, I. Moreels, P. Borri and W. Langbein, *Phys. Rev. B: Condens. Matter Mater. Phys.*, 2015, **91**, 121302.
11 A. Polovitsyn, Z. Dang, J. L. Movilla, B. Martín-García, A. H. Khan, G. H. V. Bertrand, R. Brescia and I. Moreels, *Chem. Mater.*, 2017, **29**, 5671–5680.
12 A. W. Achtstein, O. Marquardt, R. Scott, M. Ibrahim, T. Riedl, A. V. Prudnikau, A. Antanovich, N. Owschimikow, J. K. N. Lindner, M. Artemyev and U. Woggon, *ACS Nano*, 2018, **12**, 9476–9483.
13 C. She, I. Fedin, D. S. Dolzhnikov, A. Demortière, R. D. Schaller, M. Pelton and D. V. Talapin, *Nano Lett.*, 2014, **14**, 2772–2777.
14 J. Q. Grim, S. Christodoulou, F. Di Stasio, R. Krahne, R. Cingolani, L. Manna and I. Moreels, *Nat. Nanotechnol.*, 2014, **9**, 891–895.
15 M. Li, M. Zhi, H. Zhu, W.-Y. Wu, Q.-H. Xu, M. Hyphong Jhon and Y. Chan, *Nat. Commun.*, 2015, **6**, 8513.
16 R. Scott, A. W. Achtstein, A. Prudnikau, A. Antanovich, S. Christodoulou, I. Moreels, M. Artemyev and U. Woggon, *Nano Lett.*, 2015, **15**, 4985–4992.
17 J. Heckmann, R. Scott, A. V. Prudnikau, A. Antanovich, N. Owschimikow, M. Artemyev, J. I. Climente, U. Woggon, N. B. Grosse and A. W. Achtstein, *Nano Lett.*, 2017, **17**, 6321–6329.
18 R. Scott, J. Heckmann, A. V. Prudnikau, A. Antanovich, A. Mikhailov, N. Owschimikow, M. Artemyev, J. I. Climente, U. Woggon, N. B. Grosse and A. W. Achtstein, *Nat. Nanotechnol.*, 2017, 1155–1160.
19 D.-E. Yoon, W. D. Kim, D. Kim, D. Lee, S. Koh, W. K. Bae and D. C. Lee, *J. Phys. Chem. C*, 2017, **121**, 24837–24844.
20 L. Biadala, F. Liu, M. D. Tessier, D. R. Yakovlev, B. Dubertret and M. Bayer, *Nano Lett.*, 2014, **14**, 1134–1139.
21 E. V. Shornikova, L. Biadala, D. R. Yakovlev, V. F. Sapega, Y. G. Kusrayev, A. A. Mitioglu, M. V. Ballottin, P. C. M. Christianen, V. V. Belykh, M. V. Kochiev, N. N. Sibeldin, A. A. Golovatenko, A. V. Rodina, N. A. Gippius, A. Kuntzmann, Y. Jiang, M. Nasilowski, B. Dubertret and M. Bayer, *Nanoscale*, 2018, **10**, 646–656.
22 R. Scott, A. W. Achtstein, A. V. Prudnikau, A. Antanovich, L. D. A. Siebbeles, M. Artemyev and U. Woggon, *Nano Lett.*, 2016, **16**, 6576–6583.
23 R. Benchamekh, N. A. Gippius, J. Even, M. O. Nestoklon, J.-M. Jancu, S. Ithurria, B. Dubertret, A. L. Efros and P. Voisin, *Phys. Rev. B: Condens. Matter Mater. Phys.*, 2014, **89**, 035307.
24 M. Richter, *Phys. Rev. Mater.*, 2017, **1**, 016001.
25 F. Rajadell, J. I. Climente and J. Planelles, *Phys. Rev. B*, 2017, **96**, 035307.
26 S. Christodoulou, J. I. Climente, J. Planelles, R. Brescia, M. Prato, B. Martin-Garcia, A. H. Khan and I. Moreels, *Nano Lett.*, 2018, **18**, 6248–6254.
27 R. Scott, S. Kickhofel, O. Schoeps, A. Antanovich, A. Prudnikau, A. Chuvilin, U. Woggon, M. Artemyev and A. W. Achtstein, *Phys. Chem. Chem. Phys.*, 2016, **18**, 3197–3203.
28 A. G. Kelly, T. Hallam, C. Backes, A. Harvey, A. S. Esmaeily, I. Godwin, J. Coelho, V. Nicolosi, J. Lauth, A. Kulkarni, S. Kinge, L. D. A. Siebbeles, G. S. Duesberg and J. N. Coleman, *Science*, 2017, **356**, 69–73.
29 A. W. Achtstein, A. V. Prudnikau, M. V. Ermolenko, L. I. Gurinovich, S. V. Gaponenko, U. Woggon, A. V. Baranov, M. Y. Leonov, I. D. Rukhlenko, A. V. Fedorov and M. V. Artemyev, *ACS Nano*, 2014, **8**, 7678–7686.
30 A. Chu, C. Livache, S. Ithurria and E. Lhuillier, *J. Appl. Phys.*, 2018, **123**, 035701.
31 A. Prudnikau, A. Chuvilin and M. Artemyev, *J. Am. Chem. Soc.*, 2013, **135**, 14476–14479.
32 A. V. Antanovich, A. V. Prudnikau, D. Melnikau, Y. P. Rakovich, A. Chuvilin, U. Woggon, A. W. Achtstein and M. V. Artemyev, *Nanoscale*, 2015, **7**, 8084–8092.
33 Y. Kelestemur, B. Guzelturk, O. Erdem, M. Olutas, K. Gungor and H. V. Demir, *Adv. Funct. Mater.*, 2016, **26**, 3570–3579.
34 E. V. Shornikova, L. Biadala, D. R. Yakovlev, D. Feng, V. F. Sapega, N. Flipo, A. A. Golovatenko, M. A. Semina, A. V. Rodina, A. A. Mitioglu, M. V. Ballottin, P. C. M. Christianen, Y. G. Kusrayev, M. Nasilowski, B. Dubertret and M. Bayer, *Nano Lett.*, 2018, **18**, 373–380.

 This journal is © The Royal Society of Chemistry 2019

Open Access Article. Published on 30 January 2019. Downloaded on 3/28/2024 5:50:57 PM.
This article is licensed under a Creative Commons Attribution-NonCommercial 3.0 Unported Licence.

35 R. Pandya, R. Y. S. Chen, A. Cheminal, M. Dufour, J. M. Richter, T. H. Thomas, S. Ahmed, A. Sadhanala, E. P. Booker, G. Divitini, F. Deschler, N. C. Greenham, S. Ithurria and A. Rao, *J. Am. Chem. Soc.*, 2018, **140**, 14097–14111.
36 J. Zhao, J. A. Bardecker, A. M. Munro, M. S. Liu, Y. Niu, I.-K. Ding, J. Luo, B. Chen, A. K.-Y. Jen and D. S. Ginger, *Nano Lett.*, 2006, **6**, 463–467.
37 Y. Zeng and D. F. Kelley, *J. Phys. Chem. C*, 2016, **120**, 17853–17862.
38 M. Nasilowski, P. Spinicelli, G. Patriarche and B. Dubertret, *Nano Lett.*, 2015, **15**, 3953–3958.
39 K. Gong, J. E. Martin, L. E. Shea-Rohwer, P. Lu and D. F. Kelley, *J. Phys. Chem. C*, 2015, **119**, 2231–2238.
40 M. Cirillo, T. Aubert, R. Gomes, R. Van Deun, P. Emplit, A. Biermann, H. Lange, C. Thomsen, E. Brainis and Z. Hens, *Chem. Mater.*, 2014, **26**, 1154–1160.
41 C. Gollner, J. Ziegler, L. Protesescu, D. N. Dirin, R. T. Lechner, G. Fritz-Popovski, M. Sytnyk, S. Yakunin, S. Rotter, A. A. Yousefi Amin, C. Vidal, C. Hrelescu, T. A. Klar, M. V. Kovalenko and W. Heiss, *ACS Nano*, 2015, **9**, 9792–9801.
42 C. Lin, K. Gong, D. F. Kelley and A. M. Kelley, *ACS Nano*, 2015, **9**, 8131–8141.
43 J. Cui, A. P. Beyler, I. Coropceanu, L. Cleary, T. R. Avila, Y. Chen, J. M. Cordero, S. L. Heathcote, D. K. Harris, O. Chen, J. Cao and M. G. Bawendi, *Nano Lett.*, 2016, **16**, 289–296.
44 G. H. V. Bertrand, A. Polovitsyn, S. Christodoulou, A. H. Khan and I. Moreels, *Chem. Commun.*, 2016, **52**, 11975–11978.
45 S. Ithurria and D. V. Talapin, *J. Am. Chem. Soc.*, 2012, **134**, 18585–18590.
46 N. Tschirner, H. Lange, A. Schliwa, A. Biermann, C. Thomsen, K. Lambert, R. Gomes and Z. Hens, *Chem. Mater.*, 2012, **24**, 311–318.
47 M. D. Tessier, L. Biadala, C. Bouet, S. Ithurria, B. Abecassis and B. Dubertret, *ACS Nano*, 2013, **7**, 3332–3340.
48 L. Vina, S. Logothetidis and M. Cardona, *Phys. Rev. B: Condens. Matter Mater. Phys.*, 1984, **30**, 1979–1991.
49 K. P. O'Donnell and X. Chen, *Appl. Phys. Lett.*, 1991, **58**, 2924–2926.
50 J. Feldmann, G. Peter, E. O. Göbel, P. Dawson, K. Moore, C. Foxon and R. J. Elliott, *Phys. Rev. Lett.*, 1987, **59**, 2337–2340.
51 A. Riedinger, F. D. Ott, A. Mule, S. Mazzotti, P. N. Knusel, S. J. P. Kress, F. Prins, S. C. Erwin and D. J. Norris, *Nat. Mater.*, 2017, **16**, 743–748.
52 S. Helmrich, R. Schneider, A. W. Achtstein, A. Arora, B. Herzog, S. M. de Vasconcellos, M. Kolarczik, O. Schöps, R. Bratschitsch, U. Woggon and N. Owschimikow, *2D Mater.*, 2018, **5**, 045007.
53 F. Cadiz, E. Courtade, C. Robert, G. Wang, Y. Shen, H. Cai, T. Taniguchi, K. Watanabe, H. Carrere, D. Lagarde, M. Manca, T. Amand, P. Renucci, S. Tongay, X. Marie and B. Urbaszek, *Phys. Rev. X*, 2017, **7**, 021026.
54 Z. Ning, H. Tian, H. Qin, Q. Zhang, H. Ågren, L. Sun and Y. Fu, *J. Phys. Chem. C*, 2010, **114**, 15184–15189.
55 L. Wang, K. Nonaka, T. Okuhata, T. Katayama and N. Tamai, *J. Phys. Chem. C*, 2018, **122**, 12038–12046.
56 T. Takagahara, *Phys. Rev. Lett.*, 1993, **71**, 3577–3580.
57 S. A. Cherevkov, A. V. Fedorov, M. V. Artemyev, A. V. Prudnikau and A. V. Baranov, *Phys. Rev. B: Condens. Matter Mater. Phys.*, 2013, **88**, 041303.
58 B. K. Basu, *Theory of Optical Processes in Semiconductors*, Oxford Univ. Press, Oxford, 1997.
59 C. Ndebeka-Bandou, F. Carosella and G. Bastard, *Quantum States and Scattering in Semiconductor Nanostructures*, World Scientiffic, 2016.
60 A. Girard, L. Saviot, S. Pedetti, M. D. Tessier, J. Margueritat, H. Gehan, B. Mahler, B. Dubertret and A. Mermet, *Nanoscale*, 2016, **8**, 13251–13256.
61 W. Shen and S. Shen, *Infrared Phys. Technol.*, 1996, **37**, 655–657.
62 S. Shree, M. Semina, C. Robert, B. Han, T. Amand, A. Balocchi, M. Manca, E. Courtade, X. Marie, T. Taniguchi, K. Watanabe, M. M. Glazov and B. Urbaszek, *Phys. Rev. B*, 2018, **98**, 035302.
63 D. O. Sigle, J. T. Hugall, S. Ithurria, B. Dubertret and J. J. Baumberg, *Phys. Rev. Lett.*, 2014, **113**, 087402.
64 A. Antanovich, A. W. Achtstein, A. Matsukovich, A. Prudnikau, P. Bhaskar, V. Gurin, M. Molinari and M. Artemyev, *Nanoscale*, 2017, **9**, 18042–18053.
65 R. Bhargava, *Properties of Wide Bandgap II-VI Semiconductors*, INSPEC, Institute of Electrical Engineers, 1997.
66 A. M. Kelley, *ACS Nano*, 2011, **5**, 5254–5262.
67 C. Chia, C. Yuan, J. Ku, S. Yang, W. Chou, J. Juang, S. Hsieh, K. Chiu, J. Hsu and S. Jeng, *J. Lumin.*, 2008, **128**, 123–128.